International Journal of Biological Macromolecules 45 (2009) 206–212

Contents lists available at ScienceDirect

International Journal of Biological Macromolecules

journal homepage: www.elsevier.com/locate/ijbiomac

Large scale structure of wheat, rice and potato starch revealed by ultra small angle X-ray diffraction

Ekrem Dündar[a,b,*], Yusuf Turan[a], Allen E. Blaurock[c]

[a] Balıkesir Üniversitesi, Fen Edebiyat Fakültesi, Biyoloji Bölümü, 10145 Balıkesir, Turkey
[b] Illinois Institute of Technology, Department of Biological, Chemical and Physical Sciences, Chicago, IL 60616, USA
[c] Kraft Inc., Gen Foods, 801 Waukegan Rd, Glenview, IL 60025, USA

ARTICLE INFO

Article history:
Received 27 November 2008
Received in revised form 8 May 2009
Accepted 11 May 2009
Available online 20 May 2009

Keywords:
Ultra small angle X-Ray diffraction
Starch structure

ABSTRACT

Rice, wheat, and potato starches were investigated using ultra-small angle X-Ray diffraction (USXRD) in the range of 100–58,000 Å. The results showed trends consistent with the known sizes of starches. However, the observed Rg values for the scattering substances lie in the 100–300 nm range, very much in the low end of the known starch granule size distributions (and below the resolution of the light microscope) suggesting different, perhaps interesting, structures than those observed by light microscopy. Thus what were detected may possibly be the sizes of the crystalline regions postulated to occur in individual starch granules.

1. Introduction

Starch, the main storage polysaccharide in plants, is made of glucose molecules which attach to one another with α-D-(1 → 4) and α-D-(1 → 6) glycoside bonds. This macromolecule contains two different subunits called amylose and amylopectin [1,2]. Starches are distributed widely throughout plants but particularly they are stored in the seeds and in roots or tubers. In the leaves and stems of plants, the starch granules are closely associated with the green chloroplasts, where photosynthesis occurs [3]. During refining processes, the extraneous plant structures are separated from the small, rodlike (banana), spherical (corn), disk-shaped (wheat), or egg-shaped (potato) particles [4–6]. Commercial corn, potato, or other starch powders consist of these particles [1,7,8].

By ordinary microscopic observation it can be seen that granules possess a faintly visible layered structure, similar on a small scale to that of an onion, the annual rings of a tree, or the layers of a shell [1]. When the granule is excessively dried, or when attempts are made to crush the granule, it has a tendency to split radially, i.e., along lines from the center to the periphery. Study of the granules with polarized light helps to understand why this radial splitting occurs. With polarized light, the granule can be shown to have the ability to refract light doubly or to tilt light and the way in which this double refraction occurs suggests the idea that the long chainlike starch macromolecules are oriented radially in the granule [4].

X-ray diffraction is another technique that is widely used to study the starch structure. The parallel molecular chains in the granule appear to be arranged with a regularity of structure surpassing that of a simple molecular orientation, since the starch granules diffract X-rays nicely [2,8,9,10]. In other words, the parallel chains occasionally have crystalline arrangements in local regions of submicroscopic size [1,2], that makes X-ray diffraction a suitable approach to study starch.

Colloidal dimensions (between tens and several thousand Å) are enormously large compared to the X-ray wave length (e.g. the frequently used CuKα-line of 1.54 Å) which makes the angular range of observable scattering correspondingly small. Inhomogeneities in electron density of colloidal size in the sample causes small angle X-ray scattering [11]. Detailed analysis based on modeling and scattering curve for different starch granules have been reported [12]. By using lamellar microemulsion system as a point of reference, model analysis of the SAXS data were used to quantitatively characterize the lamellar structure of starch [13]. For randomly dispersed particles in solution or in a matrix, the data are radially symmetric around the incident beam, so it is only necessary to collect data along a line (in the case of conventional geometry (Fig. 12), or over an arc (in the case of an angle sensitive measurement (Fig. 13). Sampling of the pattern, however, is not continuous but occurs at discrete points by the process of digitizing the data.

Starch granules typically have dimensions exceeding 10,000 Å, much larger than the dimensions accessible (∼1000 Å) with the conventional X-ray setup described above. To access the ultra small angles required for the study of micrometer-scale structures, one

* Corresponding author at: Balıkesir Üniversitesi, Fen Edebiyat Fakültesi, Biyoloji Bölümü, 10145 Balıkesir, Turkey. Tel.: +90 266 612 1278/537 624 4220; fax: +90 266 612 1215.
E-mail addresses: dundar@balikesir.edu.tr, ekremdundar1@yahoo.com (E. Dündar).

0141-8130/$ – see front matter © 2009 Elsevier B.V. All rights reserved.
doi:10.1016/j.ijbiomac.2009.05.002

may use a Bonse–Hart camera [14,15]. In this geometry (Fig. 13), a channel-cut germanium crystal monochromator is used to direct a very well collimated X-ray beam of well-defined wavelength onto the sample. The scattered X-rays, instead of being imaged on a detector, are directed onto a second channel-cut monochromator, which is scanned over the range of accessible scattering angles. The intensity at a particular Bragg angle (2θ) is measured directly using a scintillation counter. Because the pattern is taken as a function of angle, the beam width has no smearing effect. The energy spread of the monochromatic beam is also small since essentially only the CuKα emission line from the target is accepted. Thus, at least for initial analysis, the only correction necessary is the one for the length of the beam, thereby simplifying the calculation.

A Bonse–Hart camera of this type was utilized in this study to investigate a size regime for starch particles that was formerly inaccessible using X-ray diffraction. In order to accomplish this goal we have acquired and adapted existing analysis tools to a novel application (see Section 2). Then we surveyed potato and some starch-bearing seed grains (wheat and rice) to see if they could potentially yield interpretable data using this technique.

2. Materials and methods

2.1. Ultra small angle X-ray diffraction experiments

Samples of various cereal seeds and polystyrene microspheres (Table 1) were mounted in a sample holder and scanned using a Bonse–Hart type camera [15]. The camera was mounted on a rotating-anode generator (RU200; Rigaku USA Inc., Danvers, MA) employing a 0.2 mm × 2 mm focus. Starting at an angle well away from the direct beam, the sample diffraction was scanned in 2θ, stepwise across the main beam to a comparable angle on the other side of the direct beam. The counting time per step was 1 second, but this time could be lengthened in order to improve the counting statistics. The step width varied; the smallest value was 4 arcsec while the largest value was 20 arcsec, in units of 2θ. The K-α1 and K-α2 lines from a copper target were selected by the defining channel-cut Ge crystal. Coordinated data collection and scanning of the analyzer crystal was done by using a Databox (Radix Inc. Chicago, USA).

Cereal samples were obtained from a local natural foods market. All of the scans (Table 1) were conducted twice; once with a copper foil in front of the sample to attenuate the direct beam, and a second time without the copper foil in order to improve the precision of the weaker scattering. By comparing the scans with and without a sample in place, one can observe the contribution of the main beam to the diffraction from the sample. Here the scans where Cu foil was not placed in front of the beam were used since these scans will yield more precise diffraction at larger angles.

In order to make best use of the available X-ray flux, several seeds were stacked up along the length of the direct beam. Scans were recorded with the seeds in two different orientations. In both orientations, the long dimension of the direct beam was parallel to the hilum. In the one orientation, the direct beam was incident directly onto the hilum. To obtain the other orientation, the seeds were rotated by 90° about their long axis. No difference was seen between these orientations and the patterns with the best counting statistics are shown in the results.

Images of the starch grains from potato, wheat and rice were obtained by an Olympus BX50 Phase Contrast Binocular Microscope with a camera lucida after staining with Lugol's iodine. Samples were obtained from local markets and their hydration levels are known as around 13–14% for rice, about 8% for wheat, and about 80% for potato.

Table 1
Description of experimental scans.

Sample	Description of the diffraction experiments
Sphere1	Polystyrene microspheres of 0.358 μm, no Cu foil used
Sphere2	Polystyrene microspheres of 0.481 μm, no Cu foil used
Sphere3	Polystyrene microspheres of 0.765 μm, no Cu foil used
Potato	∼3 mm thick slice, no Cu foil used
Wheat	6 Wheat berries stacked one above the other, no Cu foil used
Rice	4 Rice grains stacked one above the other, no Cu foil used

2.2. Desmearing the data

To obtain enough diffraction intensity using conventional laboratory-based X-ray sources, it is often necessary to use a line X-ray source. The difficulty with this technique is that patterns that would be circularly symmetric from a point source are convoluted with the shape of the line, with a consequent loss of detail in the X-ray pattern as well as shifts in the position of significant diffraction features. Desmearing small angle data, i.e. deconvoluting the data, is a difficult computational problem [16–18]. Glatter have produced a well established computer software package, ITR, suitable for this problem [19]. With this software it was possible to attempt to desmear the data. There is a very significant learning curve attached to using these programs since the experimental geometry assumed by the authors is not identical to the one used in the present experiments.

In the present work, the program was tested by taking data from polystyrene spheres with measured average diameters ranging from 0.358 to 0.765 μm in diameter. The beam dimensions were measured directly from a film image at a known distance from the source, which allowed the width and height to be expressed in terms of diffraction angle, and hence in hours. After confirming that the program was operating properly for the polystyrene spheres, with the Bonse–Hart setup, the program was used to desmear the data from the unknown samples.

2.3. Analysis of guinier plots

Microsoft Excel, Version 5.0 (Microsoft, Inc.) was utilized to analyze the Guinier Plots. For this, the same region used to calculate the slope, was used to find the standard error of the slope and hence the radius of gyration and its error. After running the "regression" tool of Microsoft Excel (Microsoft, Inc.), for the range mentioned, the error percentage was obtained by dividing the "standard error" value of the "x variable" by the "coefficient" value of the same variable. Confidence intervals of 95% were assumed in this calculation. Calculated Rg values were, then, multiplied by the percentage errors and their error ranges were obtained. Those values mentioned are shown as "±" signs after their respective values (see Section 3).

3. Results

3.1. Analysis of the scattering data

Initial experiments examined the diffraction patterns of polystyrene microspheres in order to test the program. Evaluating the effect of changing critical parameters was one of the major objectives in this process. After establishing that the program operated properly [20], diffraction patterns from rice, wheat, and potato starches were collected using USXRD and processed to yield desmeared $I(h)$ functions for each sample. Scattering data from microspheres of three different average diameters were first analyzed. Figs. 1–3 show the smeared and desmeared curves of 0.358 μm, 0.481 μm, and 0.765 μm polystyrene microspheres, respectively. After correctly desmearing diffraction patterns from microspheres of known sizes, the data from potato and the cereal

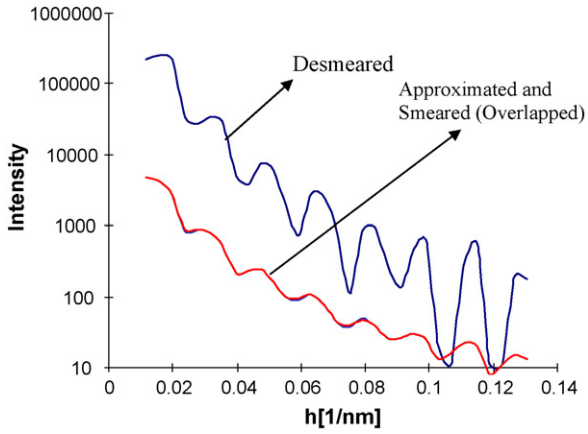

Fig. 1. Smeared, approximated, and desmeared intensity of 0.358 μm polystyrene microspheres.

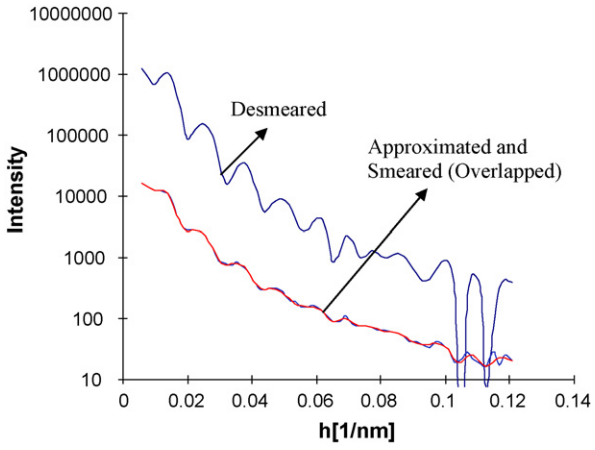

Fig. 2. Smeared, approximated, and desmeared intensity of 0.481 μm polystyrene microspheres.

grains were desmeared. Figs. 4–6 show these desmeared curves. Intensity versus *h* curves is plotted for all three data sets in Fig. 7. Data were scaled so that they had the same initial values so the shapes of the curves could be compared easily.

As seen in Fig. 7 potato starch intensity decays the fastest. When considering the reciprocal relationship of desmeared curves with

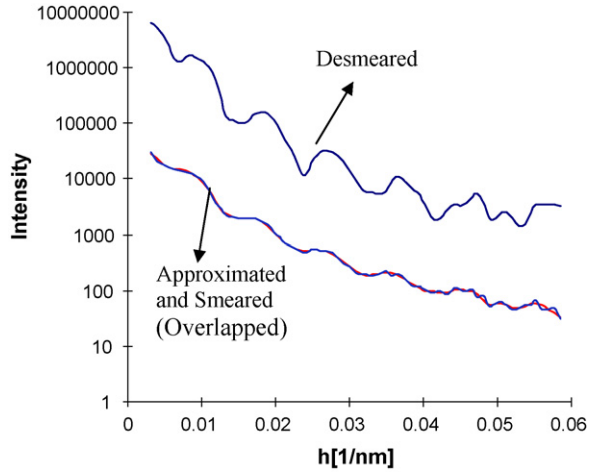

Fig. 3. Smeared, approximated, and desmeared intensity of 0.765 μm polystyrene microspheres.

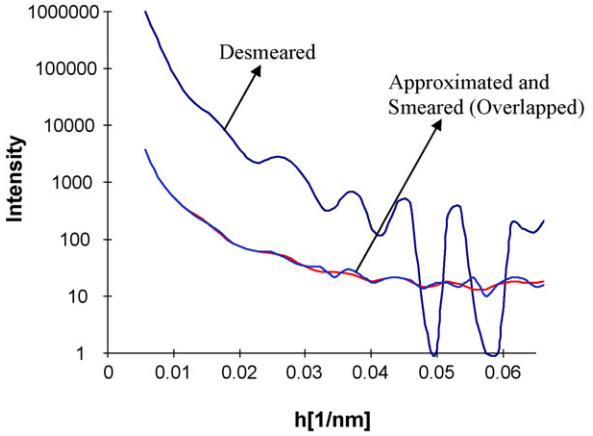

Fig. 4. Smeared, approximated, and desmeared curves of potato starch.

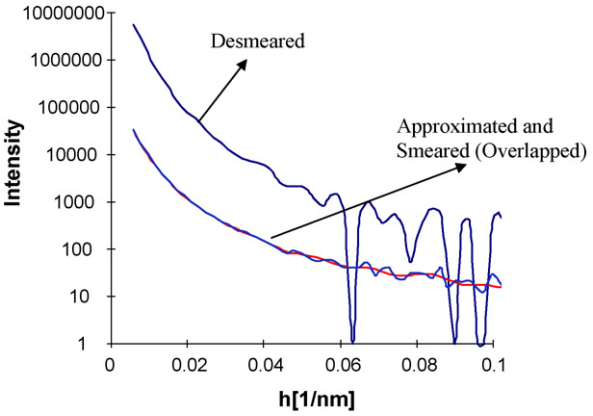

Fig. 5. Smeared, approximated, and desmeared curves of wheat starch.

the diameter of the respective particles, this is in accordance with the literature, as the potato starch has the largest diameters among the three starches mentioned [4–6]. The curves of rice and wheat have markedly similar shapes with rice initially decaying somewhat more quickly than wheat, and thereafter more slowly. It would be expected on the basis of the literature values for starch granule sizes that rice intensity would decay more slowly than wheat's, which appears to be the case at large scattering angles but not at lower angles.

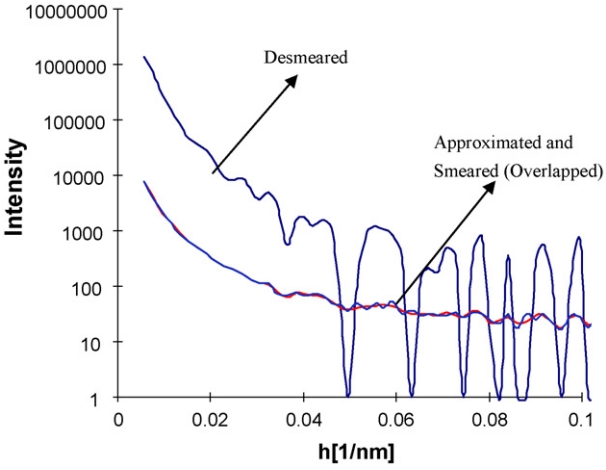

Fig. 6. Smeared, approximated, and desmeared curves of rice starch.

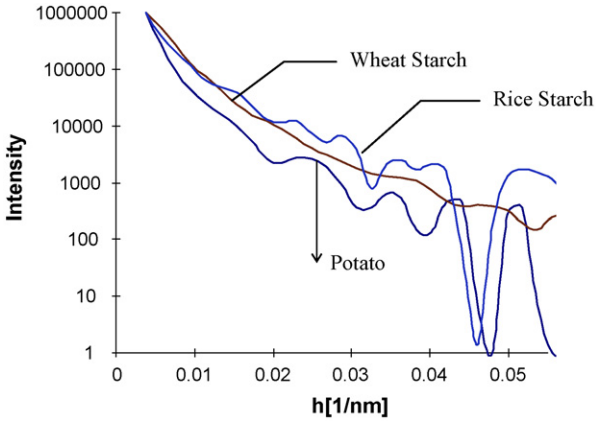

Fig. 7. Desmeared curves for potato, wheat, and rice starches.

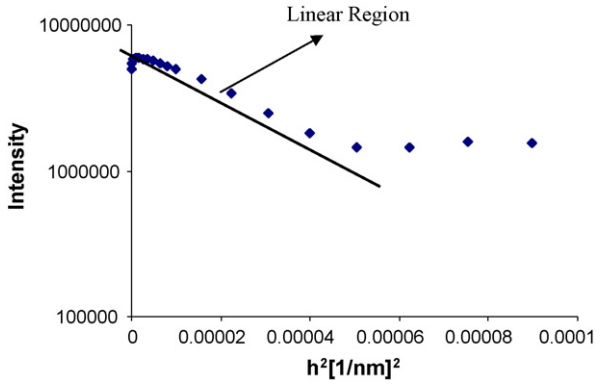

Fig. 8. Guinier plot for calculation of radius of gyration for 0.765 μm polystyrene microspheres.

3.2. Calculations of radius of gyration

Figs. 8–11 show Guinier plots for 0.765 μm polystyrene spheres, potato, wheat, and rice, respectively. As expected, the data from the 0.765 μm polystyrene spheres have a single linear region at low angles allowing one value of Rg to be calculated although the other data sets appear to have two linear regions at low angles. It was assumed that these two regions arise from two different scattering species and hence two different Rg values may be calculated.

The experimental Rg values for 0.765 μm spheres, potato starch, wheat starch, and rice starch are given in Table 2. The expected Rg for the sphere data calculated on its known radius is also given in Table 2. The expected and observed values agree within 5%.

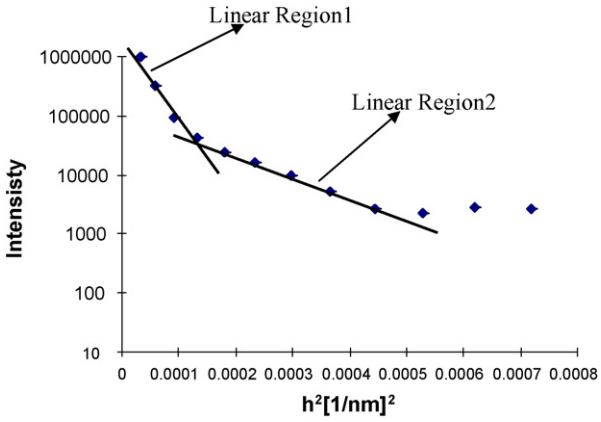

Fig. 9. Guinier plot for calculation of radius of gyration for potato starch.

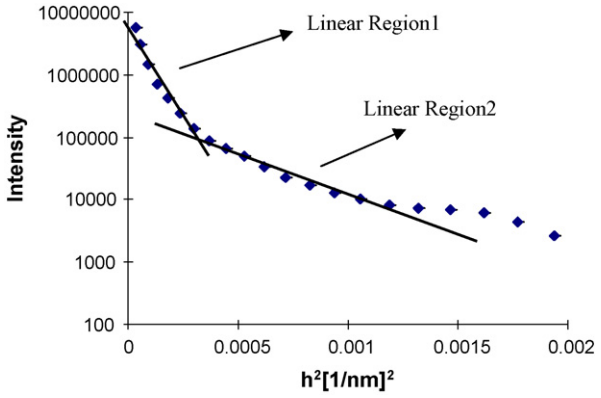

Fig. 10. Guinier plot for calculation of radius of gyration for wheat starch.

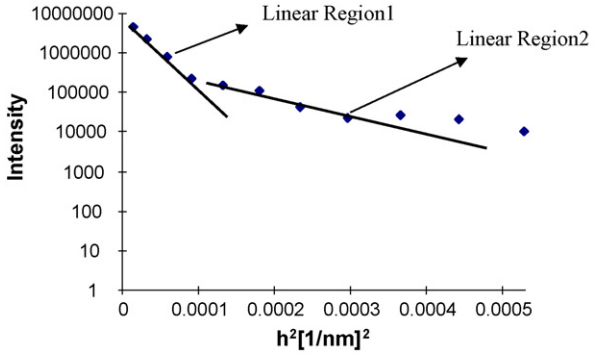

Fig. 11. Guinier plot for calculation of radius of gyration for rice starch.

Table 2
Nominal and calculated Rg values.

Sample	Calculated Rg (nm)	Nominal Rg (nm)	Deviation %
0.765 μm sphere	296.28 ± 6.9*	309	4.1
Potato starch, Rg1	308.91 ± 37.5	–	–
Potato starch, Rg2	168.70 ± 24.5		
Wheat starch, Rg1	203.70 ± 26.4	–	–
Wheat starch, Rg2	100.70 ± 4.9		
Rice starch, Rg1	299.80 ± 40.7	–	–
Rice starch, Rg2	184.50 ± 12.9		

* Errors are derived from standard error of the slope of best fit line on the Guinier plot (see Section 2).

3.3. Images of the starch granules

To display size distribution of the starch granules investigated, the images of the granules from potato, wheat and rice were obtained as described in Section 2 and are shown in Fig. 12.

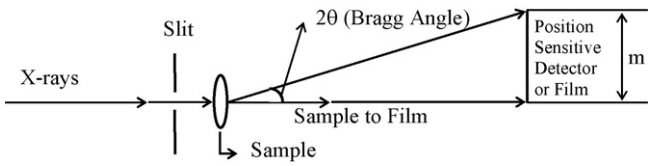

Fig. 12. The experimental geometry of a conventional X-ray camera. *m* is the distance from the center of the pattern on the film or detector.

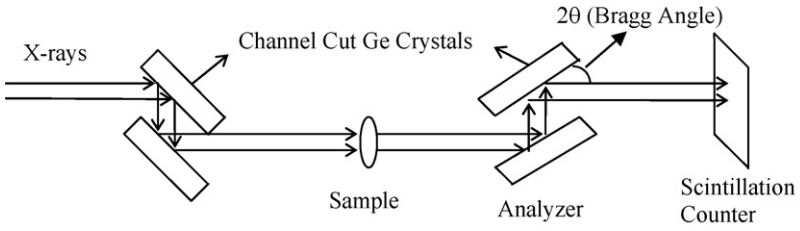

Fig. 13. The experimental geometry of a Bonse–Hart type camera.

4. Discussion

4.1. Effects that degrade experimental data

The ideal experimental design would consist of a point-like primary beam, point-like sample and detector but this can never be attained in a real experiment [11]. In order to get sufficient intensity from a laboratory based X-ray generator, it is frequently necessary to use a line shaped beam. A commonly used experimental set up is shown diagrammatically in Fig. 12. The shape of a diffraction feature on the detector at a distance m away from the main beam is altered by the non-ideal beam shape which is typically determined by a defining slit in front of the specimen. These alterations consist of the slit length effect, slit width effect and wave length effect. Some of these effects are not important in the experimental geometry used in the work (see Fig. 13), but it is important to understand this conventional experimental geometry in order to use the available software analysis packages which were written with this in mind.

Slit length effect: If the profile $Q(x)$ is infinitely narrow, a line-shaped primary beam with its intensity distribution $P(t)$ causes a smearing of the scattered intensity $I(h)$. The experimental abscissa h is a reduced angular quantity (also called q) which is related to the scattering angle 2θ by the relation $4\pi \sin\theta/\lambda$ where λ is the wave length of the radiation.

Slit width effect. In the experimental geometry shown in Fig. 12 the width of the slit defining the incident beam will cause smearing of the data incident on a detector. The slit width may be described by the intensity profile $Q(x)$, i.e. by the extension of the primary beam perpendicular to the slit length.

Wavelength effect. The smearing effect caused by a wavelength distribution $W(\lambda')$ in the primary beam can be described by the wavelength integral.

$$I\lambda(h) = \int_0^\infty W(\lambda')\, I(h/\lambda')\, d\lambda' \qquad (1)$$

where $\lambda' = \lambda/\lambda o$ is the mean wavelength used in the previous equation. Accurate experimental determination of $W(\lambda')$ is difficult, and the wavelength distribution is therefore often approximated by a sum of two delta functions (Kα and Kβ-line). The Kβ-line is excluded by the experimental geometry employed in the present work, but the angular width of the Kα line(s) may be significant on the length scales addressed in the present work (see below).

4.2. Interpretation of USXRD patterns

Once the scattering curve is desmeared, then it is possible to make direct comparisons among the various samples as well as comparing these data with theoretical curves. After this the radius of gyration can be determined from a Guinier plot [21]. The radius of gyration (Rg) is a measure of the size of the diffracting particles. To calculate the radius of gyration, it is first necessary to calculate the slope ($\Delta(\ln I)/\Delta h^2$) from the Guinier plot. After that, it can be calculated easily, using the known equation slope = Rg2/3. The relationship between the Rg and the radius spherical of particles is given as Rg2 = (3/5)R2 where R is the radius [21].

In the case of polystyrene spheres the diffraction pattern is well known both theoretically and experimentally [21]. In this case it is not necessary to determine the radius of gyration. Instead, the desmeared experimental data can directly be compared with the theoretical diffraction pattern. In particular, the radius of the spheres can be determined from the knowledge of the positions of the diffraction minima. In the case of spheres, these minima are regularly spaced, and it is this spacing that is used to derive the radius in question.

4.3. Diffraction from polystyrene microspheres

Overall, the experimental desmeared curves from various polystyrene spheres shown in Figs. 1–3 resemble the ideal diffraction pattern predicted for a solid sphere:

$$I(\phi) = F(\phi)^2 = \{4\pi R^3[\cos(\phi) - \phi\sin(\phi)]/\phi^3\}^2 \qquad (2)$$

where ϕ is equal to hR and F is the Fourier transform of the solid sphere of radius R [21]. Thus Eq. (2) predicts a regular succession of peaks separated by zeros, and these are plainly visible as peaks and minima in the desmeared curves. When the desmeared curves are examined carefully, in each case the minima are spaced regularly. This is precisely the result predicted by Eq. (2) for a uniform, solid sphere, i.e. the minima occur at increments in ϕ which are very nearly equal to π (3.1415926...). The single exception to this general rule is the distance from the center of the pattern ($2\theta = 0$) out to the first deep minimum; this distance is predicted to be nearly one-and-one-half times the regular distance between successive minima, i.e. 1.43 times π (A.E. Blaurock, unpublished calculation). Thus, one can estimate the sphere sizes by measuring the Δh between minima. Table 3 compares the nominal sphere sizes and those calculated from this analysis. The nominal and calculated sphere sizes are consistent with each other, as seen in Table 3.

It should be noted that, in each case, the desmeared curve also shows a shallower minimum between the origin and the first proper zero for a single, isolated sphere. The shallow minimum defines a small peak. There were two possibilities to account for this small peak; first, that the minimum defines the edge of the direct beam, which has not been masked out in our experiment; or second, that the small peak results from close packing of the spheres. When recorded without a specimen in place, the direct beam is in fact narrower than will account for the minimum seen in each of the desmeared curves, and therefore the first possibility is rejected. The

Table 3
Comparison of nominal and calculated sphere sizes.

Sample	Nominal size (μm)	Calculated size (μm)
Sphere1	0.358	0.397
Sphere2	0.481	0.528
Sphere3	0.765	0.883

Table 4
Comparison of expected and observed *h* values for first diffraction maxima from hexagonally close packed microspheres.

Sphere diameter (nm)	Expected *h* value (1/nm)	Observed *h* value (1/nm)
358	0.020	0.020
481	0.015	0.014
765	0.0095	0.0087

second possibility is in fact precisely what is to be expected if the spheres are packed fairly closely but without geometric regularity, i.e. increasing closeness of packing tends to suppress diffraction in the forward direction ($2\theta = 0$), thereby producing a subsidiary peak having a Bragg spacing somewhat larger than the diameter of the spheres. Table 4 shows the *h* values expected for this subsidiary maximum for each size of spheres examined along with the observed *h* values for this peak. The results bear out this interpretation.

It was possible to generate interpretable Guinier plots for 765 μm microspheres. In this case, as demonstrated in Table 2, the experimental Rg value was in very good agreement with the expected value assuring that the program was working correctly.

4.4. Diffraction from potato and selected grains

The goal here was to look for supra-molecular structure on the scale of tens of nanometers up to microns. Broadly speaking, any diffraction pattern can be divided into two parts; first, diffraction effects relating to the overall size and shape of the objects under study; and second, diffraction relating to regular, repeatable, substructure within the objects. While these two types of structure are inextricably intertwined, nonetheless it is useful to discuss them separately.

Diffraction relating to the overall size and shape can be predicted on the basis of published data relating to the shapes and sizes of the granules from the different starches examined. For two of the three types of starch studied – wheat and potato – the granules are large compared to the range of sizes accessible to the diffractometer. The larger granules in each type of seed will tend to dominate the scattering by virtue of their larger mass. Therefore in these two cases the tail end of the scattering curve from the larger granules was expected to see. In the third case, that of rice, the starch granules are comparable to the maximum size resolvable by the diffractometer, i.e. 5.77 μm. In this case, a major part of the diffraction from the granules, rather than simply the tail end of it may possible be seen. Nevertheless, the fact that the starch granule sizes in wheat and rice have a large range [5], as also can be seen in Fig. 14, suggests the possibility that the data from the rice sample contains primarily data from particles at the upper extreme of the particle size range, whereas the diffraction from the wheat sample might belong to particle sizes at the extreme lower end.

The radius of gyration data in Table 2 suggest that the structures giving rise to the small angle scattering lie in the 200–600 nm range, i.e. far below that expected for the granules (Table 2). It may be that these correspond to the low end of the starch granule size distributions and the larger diameter structures simply do not contribute to the observable diffraction. Another possibility is that the Rg values in Table 2 correspond to substructure within the granules. In particular, the crystalline regions within each granule [1] may be the source of the scattering observed, i.e. the crystalline regions may be 200–600 nm in diameter. The fact that potato and rice have very different starch granule size distributions [4–6] but have similar Rg values support this interpretation. Rg values estimated from the wheat data are substantially smaller suggesting that putative substructure in the granules, may vary among the starch bearing materials. Internal substructures of starch have also been reported based on transmission electron microscopy (called blocklet model), and are backed by recent atomic force microscopy data [22,23].

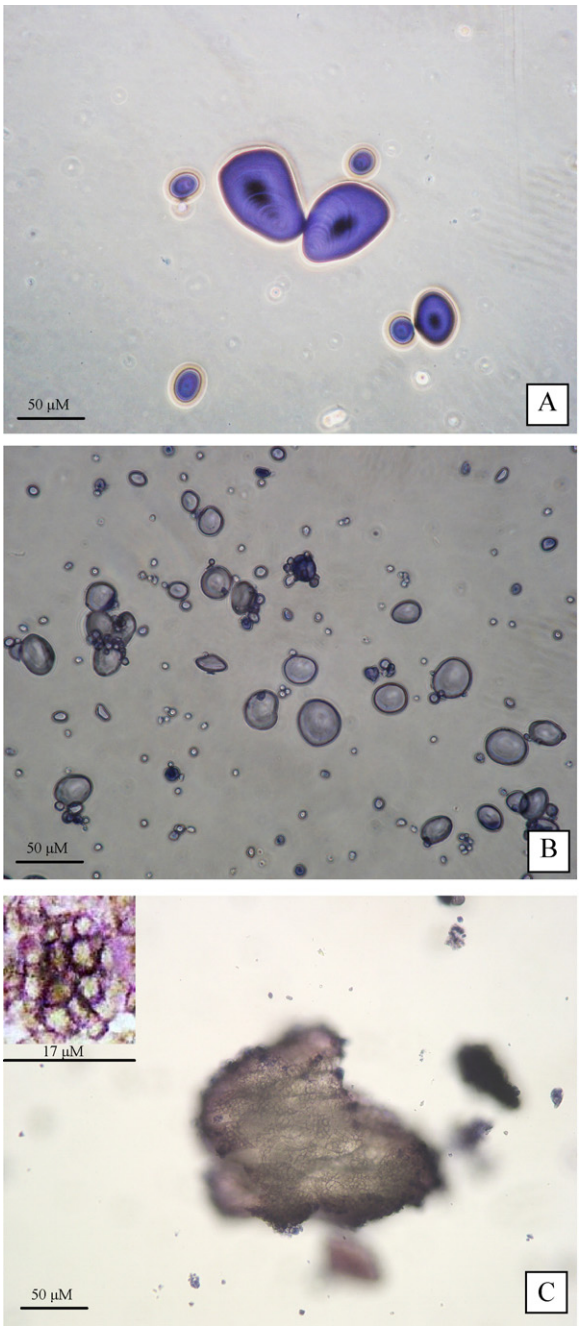

Fig. 14. Images of potato, wheat and rice starches obtained through phase contrast microscopy. (A) Potato, (B) wheat, and (C) rice.

Acknowledgement

We would like to thank Dr. Thomas C. Irving (Illinois Institute of Technology, Chicago) for his useful suggestions during and after this work.

References

[1] R.S. Bear, Tech. Rev. XLV 7 (1943) 1–6.
[2] J.P.J. Jenkins, R.E. Cameron, A.M. Donald, Starch-Starke 45 (12) (1993) 417–420.

[3] A. Buleon, P. Colonna, V. Planchot, S. Ball, Int. J. Biol. Macromol. 23 (2) (1998) 85–112.
[4] D.N. Holcomb, The Starch Granule: Current Hypothesis, Kraft Food Technology Center, Chicago, 1986, pp. 6–12.
[5] J.W. Knight, The Starch Industry, Pergamon Press, New York, 1969, p. 8.
[6] J.A. Radley, Starch and its Derivatives, Chapman & Hall Ltd., London, 1953, p. 58.
[7] J. Patindol, Y.J. Wang, J. Agric. Food Chem. 51 (2003) 2777–2784.
[8] S. Tamaki, K. Teranishi, M. Hisamatsu, T. Yamada, Starch-Starke 49 (1997) 387–390.
[9] Z. Czuchajowska, A. Klamczynski, B. Paszczynska, B.K. Baik, Cereal Chem. 75 (1998) 747–754.
[10] L.F. Wang, Y.J. Wang, R. Porter, J. Agric. Food Chem. 50 (2002) 2695–2699.
[11] O. Glatter, O. Kratky, Small Angle X-ray Scattering, Academic Press, New York, 1982, p. 276.
[12] D.R. Daniels, A.M. Donald, Biopolymers 69 (2003) 165–175.
[13] D.R. Daniels, A.M. Donald, Macromolecules 37 (2004) 1312–1318.
[14] B. Chu, Y. Li, T. Gao, Chu, Rev. Sci. Inst. 63 (1992) 4128–4133.
[15] U. Bonse, M. Hart, Z. Phys. 194 (1966) 1–17.
[16] M. Yang, J. Grider, J. Gordon, E.A. Davis, Food Microstr. 4 (1985) 107–114.
[17] J.S. Ridgen, A.N. North, A.R. Mackie, Progr. Colloid. Polym. Sci. 93 (1993) 63–65.
[18] G.D. Wignall, J.S. Lin, S. Spooner, J. Appl. Cryst. 23 (1990) 241.
[19] O. Glatter, Small Angle Scattering Software, University of Graz Press, Graz, Austria, 1993, pp. 11–150.
[20] E. Dundar, The large scale structure of some cereal starches, Master Thesis, Illinois Institute of Technology, Chicago, 1996.
[21] A. Guinier, X-Ray Diffraction in Crystals, Imperfect Crystals, and Amorphous Bodies, Freeman Press, San Fransisco, 1963, pp. 9–187.
[22] D.J. Gallant, B. Bouchet, P.M. Baldwin, Carbohydrate Polymers 32 (1997) 177–191.
[23] M.L. Parker, A.L. Kirby, V.J. Morris, Food Biophys. 3 (2008) 66–76.